COMPUTATIONAL ACOUSTICS - Volume 3
D. Lee, A. Cakmak, R. Vichnevetsky (Editors)
Elsevier Science Publishers B.V. (North-Holland)

Higher-order and elastic parabolic equations for wave propagation in the ocean

Michael D. Collins
Naval Ocean Research and Development Activity
Stennis Space Center, MS 39529

Abstract

A higher-order parabolic equation (PE) based on a Padé series [13] and an elastic PE [10] are applied to wave propagation in the ocean. In contrast to the standard PE models of underwater acoustics, the higher-order PE provides accurate solutions for problems involving arbitrarily long ranges, propagation nearly normal to the preferred direction, and large variations in sound speed. The most important applications of the higher-order PE are for problems involving elastic ocean bottoms. A new numerical approach based on centered differences is applied to handle interface conditions. The accuracy of the elastic PE is demonstrated with benchmark calculations. The elastic PE is applied to a range-dependent propagation problem.

1. Introduction

The parabolic equation [1] (PE) is very useful for wave propagation problems because it can be solved with an efficient marching algorithm. However, PE solutions are only approximate and thus are valid for only certain types of propagation problems. The original narrow-angle PE, which is based on a rational linear approximation of a square root function, is fairly accurate if the propagation direction is limited to within about 15 degrees of the preferred direction. The wide-angle PE, [2-4] which is based on a rational linear approximation of a square root function, is fairly accurate for propagation angles up to about 10 degrees. These standard versions of the PE are applicable to a large category of oceanic wave propagation problems. However, they can not handle problems involving very hard ocean bottoms or propagation very close to or very far from the sound source.

Several PE models have been derived for wave propagation in elastic media.[5-10] A few of these models were implemented and produced promising results. [5,9] However, no conclusive evidence has been provided that the elastic PE is capable of solving realistic problems. PE models that are derived by assuming that energy propagates at speeds close to a reference speed obviously can not handle problems involving coupling between compressional and shear waves. Furthermore, elastic ocean bottoms are often very hard and thus support very wide angle propagation.

To handle problems involving propagation at very wide angles or of a superposition of different wave types, a higher-order PE based on a very accurate approximation of the square root function is required. Several generalizations of the standard PE models have been investigated. [11-13] In this paper, a Padé series approximation [13] is applied to derive both acoustic and elastic PE models. Calculations are presented that demonstrate that these models are valid for propagation nearly orthogonal to the preferred direction and for wave speeds quite different from the reference speed. The results of Ref. 10 are implemented and extended: the elastic PE is generalized to

higher order and to media in which the Lamé constants and density vary continuously and solved numerically with Galerkin's method; a new numerical approach is used to handle the interface conditions between layers.

2. Standard PE approximations

We work in cylindrical coordinates with z being the depth below the ocean surface and r being the horizontal distance (range) from a time-harmonic point source of circular frequency ω. For now, the complex wavenumber $K = k + i\eta\beta \mid k \mid$ and density ρ are assumed to depend only on z, where $k = \omega/c, \beta$ is the attenuation in decibels per wavelength, c is the sound speed, and $\eta = (40\pi\log_{10}e)^{-1}$. We define the reference sound speed c_0 and reference wavenumber $k_0 = \omega/c_0$. Cylindrical spreading is handled by removing the factor $r^{-\frac{1}{2}}$ from all field variables.

For $kr >> 1$, the complex pressure P satisfies the farfield equation

$$\frac{\partial^2 P}{\partial z^2} - \frac{1}{\rho}\frac{\partial \rho}{\partial z}\frac{\partial P}{\partial z} + \frac{\partial^2 P}{\partial r^2} + K^2 P = 0, \tag{2.1}$$

which factors exactly to

$$\frac{\partial P}{\partial r} = ik_o \sqrt{1 + \frac{K^2 - k_0^2 + \frac{\partial^2}{\partial z^2} - \frac{1}{\rho}\frac{\partial \rho}{\partial z}\frac{\partial}{\partial z}}{k_0^2}}\, P. \tag{2.2}$$

By allowing K and ρ to depend on r in Eq. (2.2), which we refer to as PE_∞, a leading-order solution is obtained for problems in which range-dependence is a perturbation. [14] The exact solution of PE_∞ can be obtained in terms of outgoing coupled modes. [15]

Approximate solutions of PE_∞ are obtained by approximating the square root in Eq. (2.2) and applying numerical methods. The narrow-angle PE is obtained using the first term of the Taylor series

$$\sqrt{1+x} - 1 = \frac{1}{2}x - \frac{1}{8}x^2 + \frac{1}{16}x^3 - \ldots . \tag{2.3}$$

The plane wave factor $\exp(ik_0 r)$ is removed from P, and we assume that $K \cong k_0$ to obtain

$$\frac{\partial P}{\partial r} = i(K - k_0)P - \frac{i}{2k_0}\frac{1}{\rho}\frac{\partial \rho}{\partial z}\frac{\partial P}{\partial z} - \eta\beta \mid k_0 \mid P \quad \frac{i}{2k_0}\frac{\partial^2 P}{\partial z^2}. \tag{2.4}$$

The terms on the right side of Eq. (2.4) are the refraction term, which accounts for variations in sound speed; the density term, which accounts for density variations; the loss term, which accounts for sediment attenuation; and the diffraction term, which accounts for the vertical component of propagation.

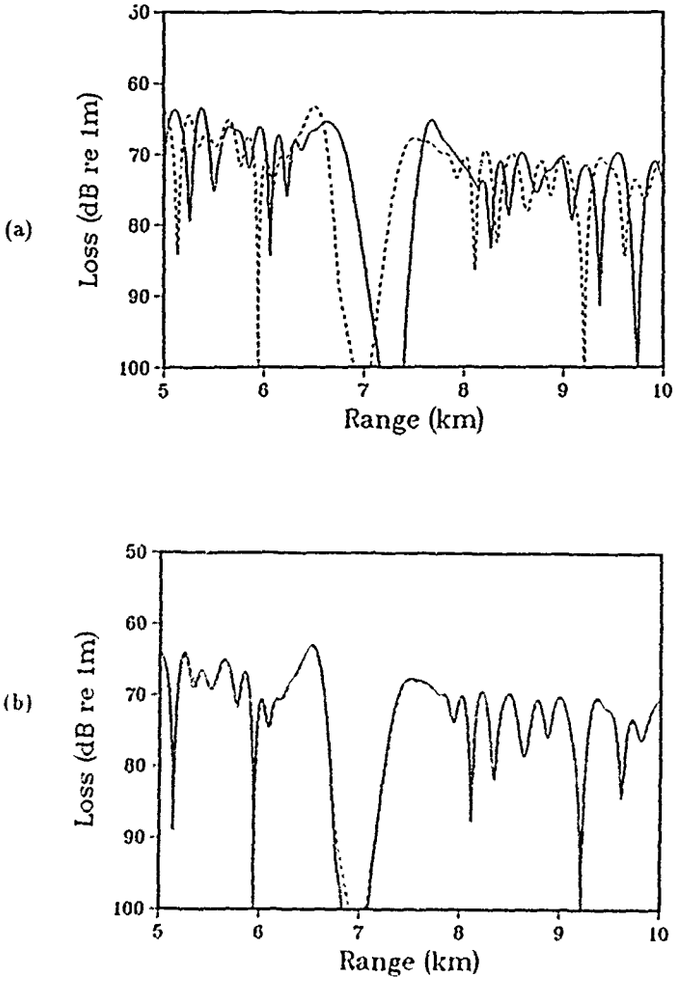

Figure 1: Transmission loss at $z = 99.5$m for NORDA Test Problem 3B. Dashed curves are the normal mode solution. Solid curves are (a) the narrow angle PE solution and (b) the wide-angle PL solution.

The narrow-angle PE is accurate only for a limited range and only if sound-speed variations and propagation angles are small. Longer ranges, larger sound speed variations, and wider propagation angles can be handled by using better approximations for the square root. The most obvious approach is to use more terms in the Taylor series. [11] Since the Taylor series diverges for $|x| > 1$, however, many terms are required for problems involving large differences in sound speed or very-wide-angle propagation. Furthermore, this approach is difficult to implement because x is raised to powers.

Table I: Comparison of Taylor and Padé series.

x	4-term Taylor	1-term Padé	2-term Padé	3-term Padé	$\sqrt{1+x}$
0.25	1.11801	1.11765	1.11803	1.11803	1.11803
0.50	1.22412	1.22222	1.22472	1.22474	1.22474
0.75	1.31870	1.31579	1.32274	1.32287	1.32288
1.00	1.39844	1.40000	1.41379	1.41420	1.41421
1.25	1.45639	1.47619	1.49904	1.49996	1.50000
1.50	1.48193	1.54545	1.57931	1.58105	1.58114
1.75	1.46078	1.60870	1.65523	1.65812	1.65831
2.00	1.37500	1.72000	1.79584	1.80221	1.80278
2.50	0.91943	1.76923	1.86124	1.86994	1.87083
2.75	0.49545	1.81481	1.92376	1.93519	1.93649
3.00	-0.10156	1.85714	1.98361	1.99817	2.00000

$$\sqrt{1+x} - 1 = \sum_{j=1}^{n} \frac{a_{j,n}x}{1+b_{j,n}x} + O(x^{2n+1}), \tag{2.5}$$

where n is the number of terms in the Padé series and

$$a_{j,n} = \frac{2}{2n+1} \sin^2 \frac{j\pi}{2n+1} \tag{2.6}$$

$$b_{j,n} = \cos^2 \frac{j\pi}{2n+1}. \tag{2.7}$$

The wide-angle PE

$$\left(3k_0^2 + K^2 + \frac{\partial^2}{\partial z^2} - \frac{1}{\rho}\frac{\partial \rho}{\partial z}\frac{\partial}{\partial z}\right) \frac{\partial P}{\partial r} = 2ik_0 \left(K^2 - k_0^2 + \frac{\partial^2}{\partial z^2} - \frac{1}{\rho}\frac{\partial \rho}{\partial z}\frac{\partial}{\partial z}\right) P \tag{2.8}$$

is based on the 1-term Padé series. The wide-angle PE does not separate into terms corresponding to simple physical processes.

We solve Eqs. (2.4) and (2.8) numerically by first discretizing depth dependence with Galerkin's method as described in the Appendix. This approach, which is valid for piecewise continuous variations in K and ρ, is easier to apply than finite difference schemes. The resulting system is then solved with Crank-Nicolson integration.

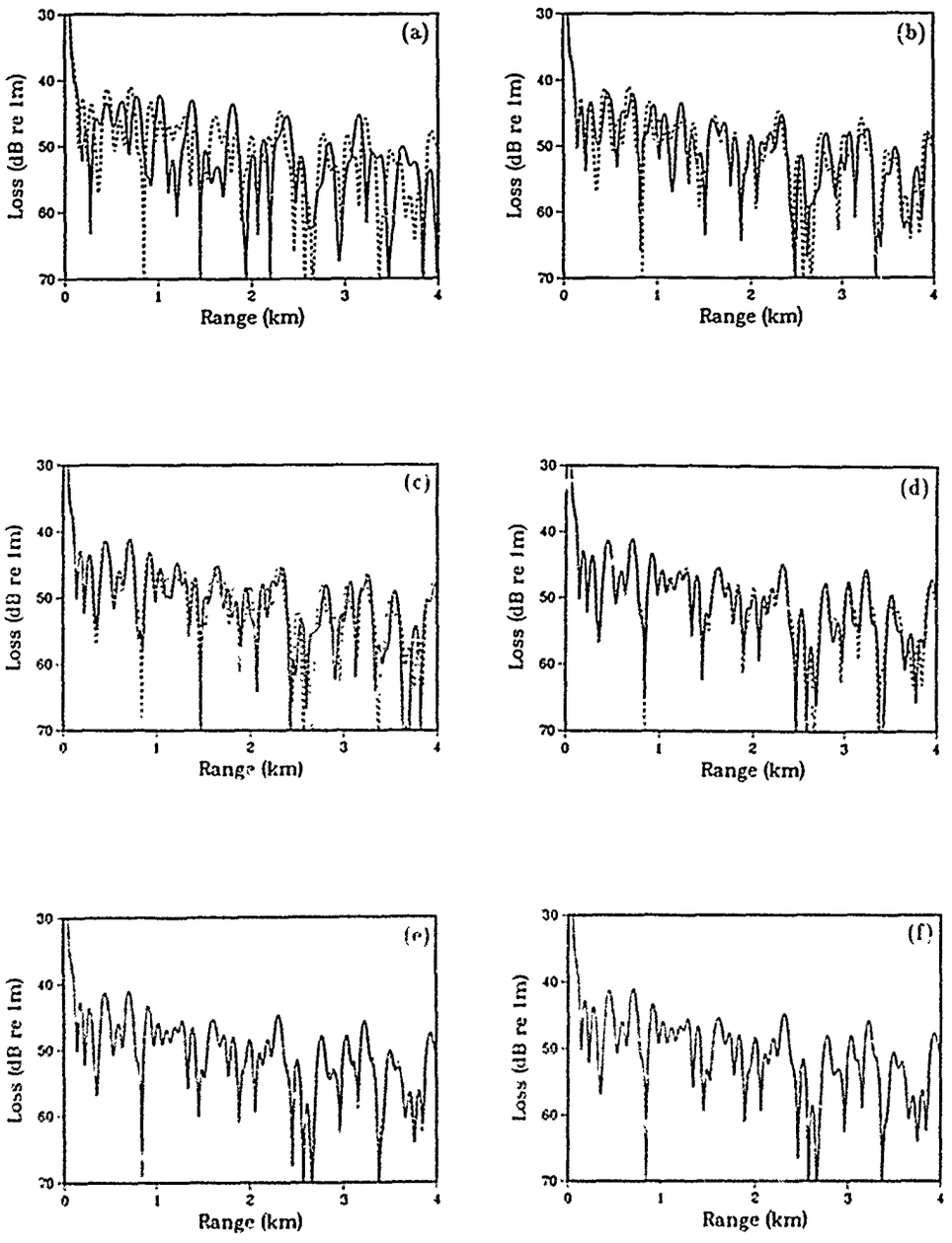

Figure 2: Transmission loss at $z = 25$m for a 25Hz source in a waveguide with perfectly reflecting boundaries. The dashed curves are the normal mode solution. The solid curves are the PE_n solution for (a) $n = 1$, (b) $n = 2$, (c) $n = 3$, (d) $n = 4$, (e) $n = 5$, and (f) $n = 6$.

We consider NORDA Test Problem 3B, [16] which involves a 250Hz source at $z = 99.5$m in an ocean 100m deep in which $c = 1500$m/s. In the sediment, $c = 1590$m/s, $\rho = 1.2$g/cm^3, and $\beta = 0.5$. We use Greene's wide-angle PE starter [4] as an initial condition at $r = 0$. The narrow-angle and wide-angle PE solutions are compared with the normal mode solution in Figure 1. The narrow-angle PE solution has a large phase error. The wide-angle PE solution is very accurate.

3. The higher-order PE

Since the Padé series is valid outside the radius of convergence of the Taylor series, relatively few terms are needed for $x \cong 1$. We illustrate this in Table I. The 4-term Taylor series is better than the 1-term Padé series for $x < 1$, but the 1-term Padé series is better for $x > 1$. The 2-term Padé series and the 4-term Taylor series are both correct to $O(x^5)$ for small x. Yet the 2-term Padé series is substantially better than the 4-term Taylor series. The 3-term Padé series is fairly accurate well beyond the radius of convergence of the Taylor series near $x = 3$.

The Padé series gives the higher-order PE

$$\frac{\partial P}{\partial r} = ik_0 \sum_{j=1}^{n} \frac{a_{j,n}\left(\frac{\partial^2}{\partial z^2} - \frac{1}{\rho}\frac{\partial \rho}{\partial z}\frac{\partial}{\partial z} + K^2 - k_0^2\right)}{k_0^2 + b_{j,n}\left(\frac{\partial^2}{\partial z^2} - \frac{1}{\rho}\frac{\partial \rho}{\partial z}\frac{\partial}{\partial z} + K^2 - k_0^2\right)} P, \tag{3.1}$$

which we refer to as PE$_n$. Equation (3.1) can be solved with the method of alternating directions. This approach involves n steps with step j requiring the solution of the equation

$$\left[k_0^2 + b_{j,n}\left(\frac{\partial^2}{\partial z^2} - \frac{1}{\rho}\frac{\partial \rho}{\partial z}\frac{\partial}{\partial z} + K^2 - k_0^2\right)\right]\frac{\partial P}{\partial r} = ik_0 a_{j,n}\left(\frac{\partial^2}{\partial z^2} - \frac{1}{\rho}\frac{\partial \rho}{\partial z}\frac{\partial}{\partial z} + K^2 - k_0^2\right) P. \tag{3.2}$$

Equation (3.2) is solved with the approach used to solve Eq. (2.8).

To illustrate the ability of PE$_n$ to handle long-range and very-wide-angle propagation, we consider a waveguide 250m thick with pressure-release top and bottom boundaries in which $c = 1500$m/s. A 25Hz point source is placed at $z = 25$m, and we take $c_0 = 1500$m/s. The eight normal modes for this problem propagate at approximately 7, 14, 21, 29, 37, 46, 57, and 74 degrees from horizontal. PE$_n$ solutions (initialized with the normal mode solution at $r = 0$) are compared with the normal mode solution in Figure 2. We observe that the PE$_n$ solutions break down very rapidly with r for small n. However, the PE$_8$ solution is very accurate at $r = 4$km.

We now consider an example that illustrates the application of PE$_n$ for low-frequency underwater acoustic propagation in deep water. In the water column, we assume the Munk profile [17]

$$c(z) = c_{ch}\left\{1 + \mu\left[2\frac{z - z_{ch}}{H} + \exp\left(-2\frac{z - z_{ch}}{H}\right) - 1\right]\right\}, \tag{3.3}$$

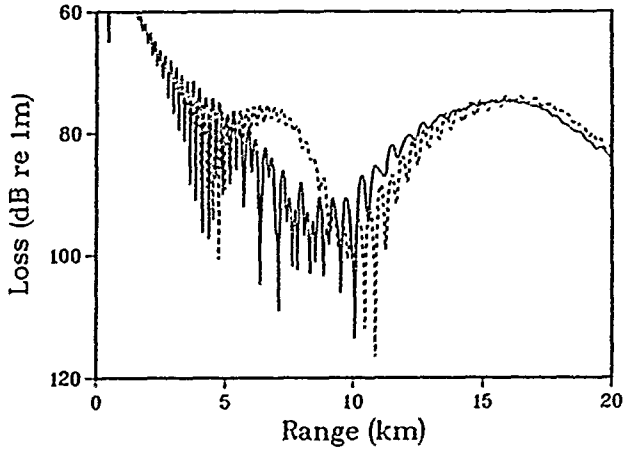

Figure 3: Transmission loss at $z = 200$m for a 10Hz source in deep water over a hard acoustic bottom. The dashed curve is the PE_1 solution. The solid curve is the PE_5 solution.

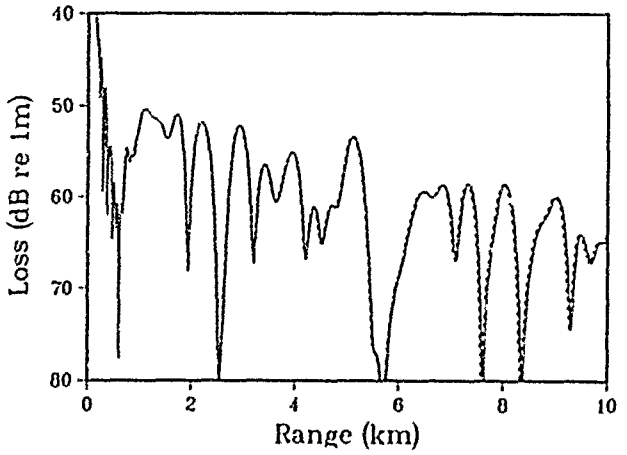

Figure 4: Transmission loss at $z = 25$m for a 50Hz source in shallow water. The dashed curve is the PE_2 solution for $c_0 = 1500$m/s. The solid curve is the PE_{15} solution for $c_0 = 300$m/s.

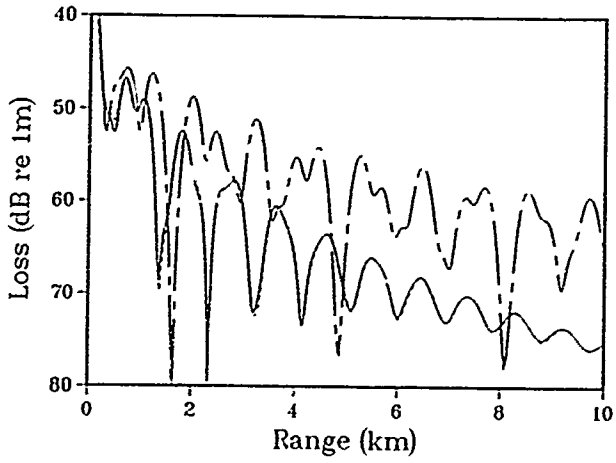

Figure 5: Transmission loss at z = 25m for a soft elastic bottom. The elastic PE solution with interface conditions (solid curve) and FFP solution (dashed curve) are in nearly perfect agreement. The acoustic PE solution (broken curve) is included to show the importance of shear effects.

where $\mu = 0.0071$, c_{ch} = 1500m/s, z_{ch} = 1000m, and H = 1200m. The ocean depth is 5000m. In the sediment, c = 1850m/s, ρ = 1.5g/cm^3, and $\beta = 0.5$. A 10Hz point source is placed at z = 200m, and we take c_0 = 1500m/s. The homogeneous half-space field [18] is used to initialize the field at r = 400m. The Lloyd's mirror beams produced by the source propagate at approximately 11, 34, and 70 degrees. PE_1 should accurately account for the 11 and 34 degree beams for well beyond r = 20km. From the PE_1 and PE_5 solutions appearing in Figure 3, however, we observe that PE_1 can not handle the 70 degree beam which is partially reflected from the ocean bottom and makes a significant contribution to the field for 5km < r <15km.

To illustrate a possible application of PE_n in elastic media, we consider a problem for which c = 1500m/s in the water and the ocean depth is 200m. In the sediment, c = 1700m/s, ρ = 1.5g/cm^3, and $\beta = 0.5$. A 50Hz point source is placed at z = 25m. The PE_2 solution for c_0 = 1500m/s and the PE_{15} solution for c_0 = 300 m/s appear in Figure 4. The agreement of the solutions suggests that a higher-order elastic PE based on the Padé series would handle both compressional and shear waves simultaneously.

4. The elastic PE

The farfield equations for the horizontal and vertical displacement u and v in an elastic medium are [19]

$$\mu\frac{\partial^2 u}{\partial r^2} + \mu\frac{\partial^2 u}{\partial z^2} + \rho\omega^2 u + (\lambda+\mu)\frac{\partial \Delta}{\partial r} + \frac{\partial \mu}{\partial z}\frac{\partial u}{\partial z} + \frac{\partial \mu}{\partial z}\frac{\partial v}{\partial r} = 0 \tag{4.1}$$

$$\mu\frac{\partial^2 v}{\partial r^2} + \mu\frac{\partial^2 v}{\partial z^2} + \rho\omega^2 v + (\lambda+\mu)\frac{\partial \Delta}{\partial z} + 2\frac{\partial \mu}{\partial z}\frac{\partial v}{\partial z} + \frac{\partial \lambda}{\partial z}\Delta = 0, \tag{4.2}$$

where the dilatation Δ is defined by

$$\Delta = \frac{\partial u}{\partial r} + \frac{\partial v}{\partial z}. \tag{4.3}$$

Loss is handled by using the complex compressional and shear speeds $c_p = \mathrm{Re}(c_p)/(1 + i\eta\beta_p)$ and $c_s = \mathrm{Re}(c_s)/(1 + i\eta\beta_s)$, where β_p and β_s are the compressional and shear attenuation and $\eta = (40\pi \log_{10} e)^{-1}$. The Lamé constants λ and μ are related to the wave speeds and the density ρ by $\lambda = \rho(c_p^2 - 2c_s^2)$ and $\mu = \rho c_s^2$.

We differentiate Eq. (4.1) with respect to r and Eq. (4.2) with respect to z and sum them using Eq. (4.3) to obtain

$$\begin{aligned}(\lambda+2\mu)\frac{\partial^2 \Delta}{\partial r^2} + (\lambda+2\mu)\frac{\partial^2 \Delta}{\partial z^2} + \rho\omega^2\Delta + 2\frac{\partial \mu}{\partial z}\frac{\partial^2 v}{\partial r^2} + \omega^2\frac{\partial \rho}{\partial z}v + \\ \left(\frac{\partial \lambda}{\partial z} + 2\frac{\partial \mu}{\partial z}\right)\frac{\partial \Delta}{\partial z} + \frac{\partial}{\partial z}\left(\frac{\partial \lambda}{\partial z}\Delta\right) + 2\frac{\partial}{\partial z}\left(\frac{\partial \mu}{\partial z}\frac{\partial v}{\partial z}\right) = 0.\end{aligned} \tag{4.4}$$

Equations (4.2) and (4.4) provide a coupled system of the form

$$L\frac{\partial^2}{\partial r^2}\begin{pmatrix}\Delta\\ v\end{pmatrix} + M\begin{pmatrix}\Delta\\ v\end{pmatrix} = 0, \tag{4.5}$$

which reduces to the formulation used in Ref. 10 for a homogeneous medium. Since the operators L and M commute with $\partial/\partial r$, we may factor Eq. (4.5) to obtain the outgoing wave equation

$$\frac{\partial}{\partial r}\begin{pmatrix}\Delta\\ v\end{pmatrix} = ik_0\sqrt{1 + \frac{L^{-1}(M - k_0^2 L)}{k_0^2}}\begin{pmatrix}\Delta\\ v\end{pmatrix}. \tag{4.6}$$

The plane wave factor $\exp(ik_0 r)$ is removed from Δ and v and the square root in Eq. (4.6) is approximated with the Padé series to obtain the higher-order elastic PE

$$\frac{\partial}{\partial r}\begin{pmatrix}\Delta\\ v\end{pmatrix} = ik_0\sum_{j=1}^{n}\frac{a_{j,n}L^{-1}(M - k_0^2 L)}{k_0^2 + b_{j,n}L^{-1}(M - k_0^2 L)}\begin{pmatrix}\Delta\\ v\end{pmatrix}. \tag{4.7}$$

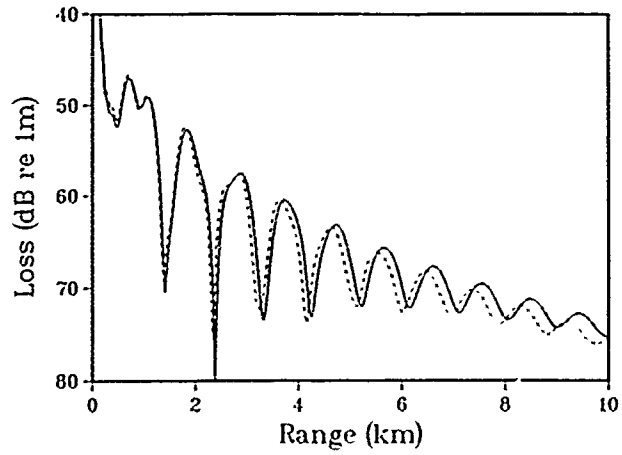

Figure 6: Transmission loss at $z = 25$m for a soft elastic bottom. The elastic PE solution with Galerkin's method for the interface (solid curve) and the FFP solution (dashed curve) are in fairly good agreement.

We solve the elastic PE numerically with the method of alternating directions and Crank-Nicolson integration to march the solution in r. The depth operators are replaced with matrices using Galerkin's method within layers in which λ, μ, and ρ are continuous as described in the Appendix. Conditions for the continuity of the displacements and the normal and tangential stresses are used at interfaces between solid layers. At a fluid-solid interface, however, horizontal displacement is not required to be continuous.

Let us consider a fluid-solid interface at $z = z_j$ (the grid points z_i are defined in the Appendix) and introduce the subscripts w and b for the fluid (water) and solid (bottom) layers. We use the physical values $\Delta_w(z_j), \Delta_b(z_j), v_b(z_j), \Delta_w(z_{j-1}), \Delta_b(z_{j+1})$, and $v_b(z_{j+1})$ and the nonphysical values $\Delta_w(z_{j+1}), \Delta_b(z_{j-1})$, and $v_b(z_{j-1})$ in the discretized equations of motion in both layers at $z = z_j$. We also use these values to form differences at $z = z_j$ for the following conditions for continuity of vertical displacement, normal stress, and tangential stress [10]:

$$\frac{\partial}{\partial z}(\lambda_w \Delta_w) + \rho_w \omega^2 v_b = 0 \tag{4.8}$$

$$\lambda_w \Delta_w = \lambda_b \Delta_b + 2\mu_b \frac{\partial v_b}{\partial z} \tag{4.9}$$

$$\frac{\partial}{\partial z}(\lambda_b \Delta_b) + 2\frac{\partial}{\partial z}(\mu_b \frac{\partial v_b}{\partial z}) + \rho_b \omega^2 v_b = 0. \tag{4.10}$$

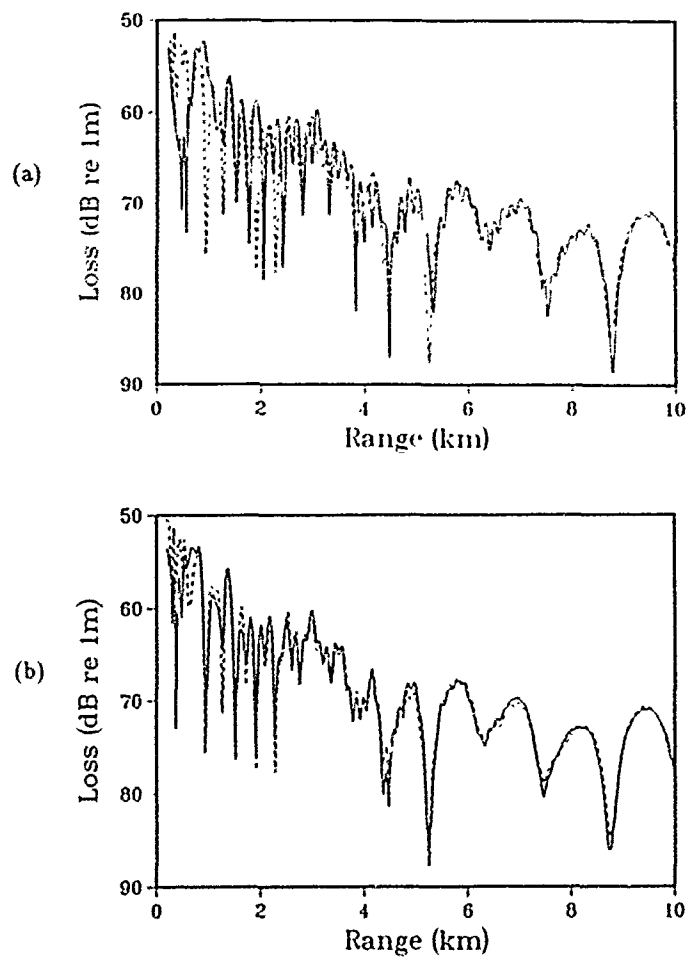

Figure 7: Transmission loss at $z = 25$m for a hard elastic bottom. The elastic PE (solid curves) and the FFP solution (dashed curves). (a) The solutions do not agree for $n = 1$. (b) The solutions are in good agreement for $n = 3$.

The nonphysical values are eliminated in the equations of motion at $z = z_j$ using the difference formulas for Eqs. (4.8), (4.9), and (4.10). A solid-solid interface is handled similarly using the interface conditions described in Ref. 10.

In a fluid medium, $P = \lambda\Delta$ can be initialized at $r = r_0$ with the homogeneous half-space field [18] P_h for a point source at $z = z_0$

$$P_h = \frac{1}{d_-} \exp\left[\frac{i\omega d_-}{c_p(z_0)}\right] - \frac{1}{d_+} \exp\left[\frac{i\omega d_+}{c_p(z_0)}\right] \tag{4.11}$$

$$d_{\pm}^2 = r_0^2 + (z \pm z_0)^2, \tag{4.12}$$

where $kr_0 >> 1$. The half-space field accounts for the direct arrival and the surface-reflected arrival. This PE starter is generalized to elastic media by applying the half-space quantities

$$\Delta_h = \frac{1}{\lambda(z_0)} P_h \tag{4.13}$$

$$v_h = -\frac{1}{\omega^2} \frac{\partial P_h}{\partial z} \tag{4.14}$$

to initialize Δ and v. This starter is valid only if the source is at least a few wavelengths away from the ocean bottom. We define transmission loss to be $-20\log_{10} | \lambda(z_0)\Delta | + 10\log_{10} r$. This definition corresponds to the usual definition of transmission loss in a homogeneous fluid.

We first consider a problem involving a 50Hz source at $z = 25$m in an ocean of depth 100m in which $c_p = 1500$m/s. In the uniform elastic sediment, $c_p = 1700$m/s, $c_s = 800$m/s, $\rho = 1$g/cm^3, $\beta_p = 0.5$, and $\beta_s = 0.5$. For the numerical solution of the elastic PE, we used the values $n = 1$, $\Delta r = 5$m, $\Delta z = 0.5$, and $r_0 = 100$m. To eliminate an instability in the numerical solution, it was necessary to extend the computational domain 2km below the ocean surface at which we assumed that both Δ and v vanish. Both the compressional and the shear attenuation were increased linearly to 10 in the lower 100m of the domain to prevent reflections. Transmission loss generated with the elastic PE and with an FFP model [20,21] appears in Figure 5. The solutions are in nearly perfect agreement.

We also performed an elastic PE calculation for this problem using the difference equations obtained with Galerkin's method to model the ocean bottom interface. This approach, which produces accurate results for acoustics problems, [22] is easier to implement. Although L^{-1} does not exist where μ vanishes, the v solution of Eq. (4.2) is also a v solution of Eq. (4.7) in a fluid. Thus the elastic PE should be valid for $\mu = 0$. We observe from the transmission loss data appearing in Figure 6 that Galerkin's method handles discontinuities fairly well. This is consistent with the discussion in Ref. 23. We deduce that Galerkin's method should handle continuous variations very well.

We now consider a problem involving a 20Hz source at $z = 25$m in an ocean of depth 600m in which $c_p = 1500$m/s. In the uniform elastic sediment, $c_p = 3400$m/s, $c_s = 1700$m/s, $\rho = 2$g/cm^3, $\beta_p = 0.5$, and $\beta_s = 0.5$. The hard ocean bottom supports very wide propagation angles in the water column. For the numerical solution of the elastic PE, we extended the computational domain to $z = 10$km and used the values $\Delta r = 10$m, $\Delta z = 1$m, and $r_0 = 200$m. The attenuation was increased linearly to 100 in the lower 1km of the domain. The elastic PE solution appears in Figure 7 for $n = 1$ and for $n = 3$. The elastic PE can not handle the wide propagation angles for $n = 1$. However, the $n = 3$ solution is in good agreement with the FFP solution.

In PE modeling, range-dependent problems are handled approximately by allowing the entries of the matrices for the depth operators to depend on range. This approach, which is easily implemented, produces accurate results for acoustics problems if range dependence is sufficiently gradual.

(a)

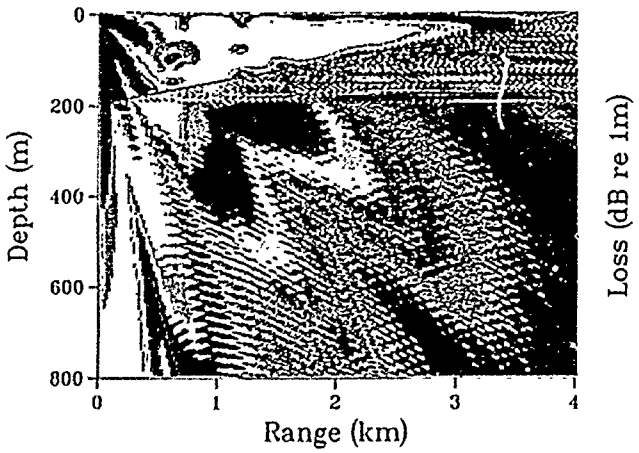

(b)

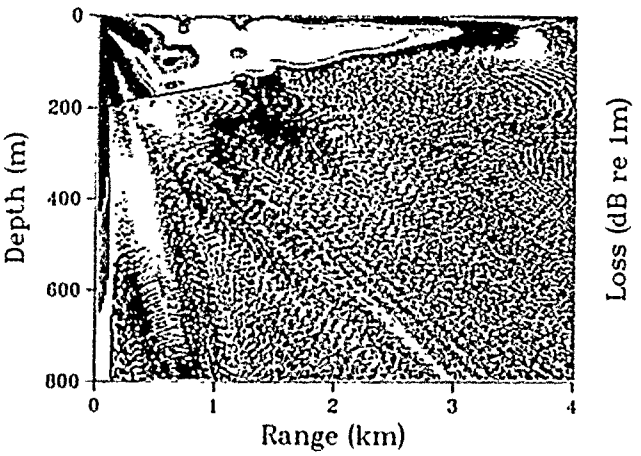

Figure 8: Transmission loss contours for a sloping elastic ocean bottom for (a) $n = 1$ and (b) $n = 10$. The black lines mark the ocean bottom.

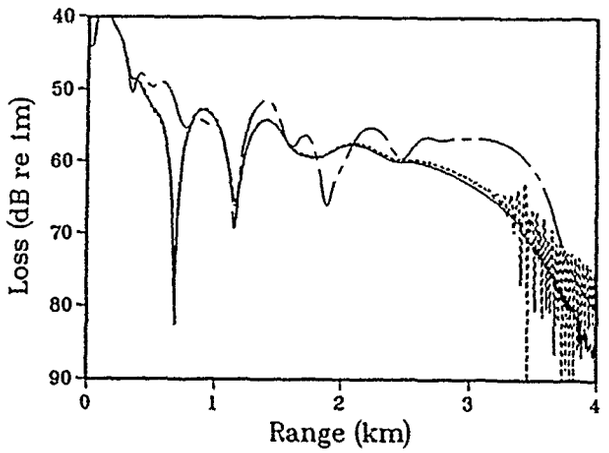

Figure 9: Transmission loss at $z = 30$m for a sloping elastic bottom. The elastic PE solution for $n = 10$ (solid curve) and $n = 1$ (dashed curve) and the acoustic PE solution (broken curve).

This approach should also be valid for weakly range-dependent problems in elastic media.

We modify a range-dependent benchmark problem [24] to illustrate the higher-order elastic PE model for a range-dependent problem. A 25Hz source is located at $z = 100$m in an ocean in which $c = 1500$m/s and the depth d is given by

$$d = \left(1 - \frac{r}{4\text{km}}\right) 200\text{m}. \tag{4.15}$$

In the sediment, $c_p = 1700$m/s, $\rho = 1.5$g/cm^3, and $\beta_p = 0.5$ for the original acoustic problem. We take $c_s = 800$m/s and $\beta_s = 0.5$. Due to the sloping ocean bottom, a significant amount of energy is transmitted into both shear and compressional waves in the bottom. Thus one might expect the $n = 1$ elastic PE to have difficulty handling this problem.

We extend the grid down to $z = 10$km and take $\Delta r = 5$m, $\Delta z = 1$m, $r_0 = 100$m, and $c_0 = 1500$m/s. Contour plots of transmission loss appear in Figure 8 for $n = 1$ and $n = 10$. The $n = 1$ solution breaks down in the sediment because it does not handle the transmitted shear waves. The $n = 10$ solution does not appear to break down in the sediment. Transmission loss curves appear in Figure 9. We observe that the elastic PE solution exhibits more loss than the acoustic PE solution and that the $n = 1$ and $n = 10$ solutions are in good agreement in the water column.

5. Conclusion

Higher-order acoustic and elastic PE models based on a Padé series have been derived and solved numerically. The higher-order PE models produce accurate solutions for propagation nearly orthogonal to the preferred direction and for large variations in sound speed. In particular, the sound speed may deviate far from the reference sound speed. The elastic PE allows hard ocean bottoms as well as continuous variations in the Lamé constants and density. It appears to handle propagation of a superposition of different types of elastic waves. Galerkin's method was used to discretize the elastic PE, which has relatively complicated depth operators. A new numerical approach was used for the interface conditions between layers. The half-space PE starter has been generalized to elastic media. Benchmark calculations demonstrate that the elastic PE and the half-space elastic PE starter produce accurate solutions for range-independent problems. The elastic PE was applied to a range-dependent problem.

The half-space starter is not valid for very low frequencies or for sources close to the ocean bottom. Since these kinds of problems involve strong coupling into shear and interface waves, an elastic PE starter that handles them would be useful. With the boundary conditions we used at the bottom of the grid, the elastic PE is stable only if the domain is truncated at a large depth. Bottom boundary conditions that allow smaller truncation depths would improve the efficiency of the model. It might be possible to accurately handle interfaces with Galerkin's method by slightly modifying the formulation of the elastic PE and/or by using different basis functions. This would improve the simplicity of the model.

Acknowledgments

This work was supported by the Office of Naval Research and the Naval Ocean Research and Development Activity. The author thanks K. Gilbert for suggesting Galerkin's method for the numerical solution of the elastic PE and H. Schmidt for the use of his FFP model for the benchmark comparisons.

References

[1] Tappert, F.D, "The Parabolic Approximation Method," in *Wave Propagation and Underwater Acoustics*, edited by J.B. Keller and J.S. Papadakis, Lecture Notes in Physics, Vol. 70, Springer, New York, 1977.

[2] Claerbout, J.F., *Fundamentals of Geophysical Data Processing*, McGraw-Hill, New York, 1976, 206-207.

[3] Botseas, G., Lee, D., and Gilbert, K.E., "IFD: Wide-Angle Capability," NUSC Tech. Rep. 6905, 1983.

[4] Greene, R.R., "The Rational Approximation to the Acoustic Wave Equation with Bottom Interaction," *J. Acoust. Soc. Am.*, 1984, 76, 1764-1773.

[5] Landers, T. and Claerbout, J.F., "Numerical Calculations of Elastic Waves in Laterally Inhomogeneous Media," *J. Geophys. Res.*, 1972, 77(8), 1476-1483.

[6] McCoy, J.J., "A Parabolic Theory of Stress Wave Propagation through Inhomogeneous Linearly Elastic Solids," 1977, 44, 462-468.

[7] Hudson, J.A., "A Parabolic Approximation for Elastic Waves," *Wave Motion*, 1980, 2, 207-214.

[8] Corones, J.P., DeFacio, B., and Krueger, R.J., "Parabolic Approximations to the Time-Independent Elastic Wave Equation," *J. Math. Phys.*, 1982, 23(4), 577-586.

[9] Wales, S.C. and McCoy, J.J., "A Comparison of Parabolic Wave Theories for Linearly Elastic Solids," *Wave Motion*, 1983, 5, 99-113.

[10] Greene, R.R., "A High-Angle One-Way Wave Equation for Seismic Wave Propagation along Rough and Sloping Interfaces," *J. Acoust. Soc. Am.*, 1985, 77, 1991-1998.

[11] St. Mary, D.F., Lee, D., and Botseas, G., "A Modified Wide Angle Wave Equation," *J. Comp. Phys.*, 1987, 71, 304-315.

[12] Knightly, G.H., Lee, D., and St. Mary, D.F., "A Higher-Order Parabolic Wave Equation," *J. Acoust. Soc. Am.*, 1987, 82, 580-587.

[13] Bamberger, A., Engquist, B., Halpern, L., and Joly, P., "Higher Order Paraxial Wave Equation Approximations in Heterogeneous Media," *SIAM J. Appl. Math.*, 1988, 48, 129-154.

[14] Jensen, F.B. and Kuperman, W.A., "Sound Propagation in a Wedge-Shaped Ocean with a Penetrable Bottom," *J. Acoust. Soc. Am.*, 1980, 67, 1564-1566.

[15] Evans, R.B., "A Coupled Mode Solution for Acoustic Propagation in a Waveguide with Stepwise Depth Variations of a Penetrable Bottom," *J. Acoust. Soc. Am.*, 1983, 74, 188-195.

[16] "NORDA Parabolic Equation Workshop," edited by J.A. Davis, D. White, and R.C. Cavanagh, NORDA Tech. Note 143, 1982.

[17] Munk, W.H., "Sound Channel in an Exponentially Stratified Ocean with Applications to SOFAR," *J. Acoust. Soc. Am.*, 1974, 55, 220-226.

[18] Collins, M.D., "A Nearfield Asymptotic Analysis for Underwater Acoustics," *J. Acoust. Soc. Am.*, 1989, 85, 1107-1114.

[19] Kolsky, H., *Stress Waves in Solids*, Dover, New York, 1963, 11.

[20] Schmidt, H. and Jensen, F.B., "A Full Wave Solution for Propagation in Multilayered Viscoelastic Media with Application to Gaussian Beam Reflection at Fluid Solid Interfaces," *J. Acoust. Soc. Am.*, 1985, 77, 813-825.

[21] Schmidt, H., "SAFARI User's Guide," SACLANT Undersea Research Centre, La Spezia, Italy, 1988.

[22] Collins, M.D., "The Time-Domain Solution of the Wide-Angle Parabolic Equation Including the Effects of Sediment Dispersion," *J. Acoust. Soc. Am.*, 1988, 84, 2114-2125.

[23] Wait, R. and Mitchell, A.R., *Finite Element Analysis and Applications*, Wiley, New York, 1985, 92-98.

[24] Collins, M.D., "Benchmark Calculations for Higher-Order Parabolic Equations," *J. Acoust. Soc. Am.*, to appear.

Appendix: Depth discretization with Galerkin's method

We define the depth grid points $z_i = i\Delta z$. The basis functions $\Psi_i(z)$ vanish for $|z - z_i| > \Delta z$, increase linearly from 0 to 1 over $z_{i-1} < z < z_i$, and decrease from 1 to 0 over $z_i < z < z_{i+1}$. We define $\Theta_i = \Theta(z_i)$ for an arbitrary coefficient function Θ and $\Phi_i = \Phi(z_i)$ for the dependent variable Φ. The basis functions provide the approximations

$$\Theta(z) \cong \sum_i \Theta_i \Psi_i(z) \tag{A.1}$$

$$\Phi(z) \cong \sum_i \Phi_i \Psi_i(z). \tag{A.2}$$

The depth operator Q_z is discretized with Galerkin's method as follows:

$$Q_z \Phi|_{z=z_i} \cong \frac{\int \Psi_i Q_z \Phi \, dz}{\int \Psi_i \, dz}. \tag{A.3}$$

Substituting Eqs. (A.1) and (A.2) into Eq. (A.3), we obtain the following approximations for the depth operators:

$$\Theta\Phi\Big|_{z=z_i} \cong \frac{\Theta_{i-1} + \Theta_i}{12} \Phi_{i-1} + \frac{\Theta_{i-1} + 6\Theta_i + \Theta_{i+1}}{12} \Phi_i + \frac{\Theta_{i+1} + \Theta_i}{12} \Phi_{i+1} \tag{A.4}$$

$$\Theta \frac{\partial \Phi}{\partial z}\Big|_{z=z_i} \cong \frac{-\Theta_{i-1} - 2\Theta_i}{6\Delta z} \Phi_{i-1} + \frac{\Theta_{i-1} - \Theta_{i+1}}{6\Delta z} \Phi_i + \frac{\Theta_{i+1} + 2\Theta_i}{6\Delta z} \Phi_{i+1} \tag{A.5}$$

$$\Theta \frac{\partial^2 \Phi}{\partial z^2}\Big|_{z=z_i} \cong \frac{\Theta_i}{(\Delta z)^2} \Phi_{i-1} - \frac{2\Theta_i}{(\Delta z)^2} \Phi_i + \frac{\Theta_i}{(\Delta z)^2} \Phi_{i+1} \tag{A.6}$$

$$\left.\frac{\partial \Theta}{\partial z}\Phi\right|_{z=z_i} \cong \frac{-\Theta_{i-1} + \Theta_i}{6(\Delta z)}\Phi_{i-1} +$$

$$\frac{\Theta_{i-1} + \Theta_{i+1}}{3\Delta z}\Phi_i + \frac{\Theta_{i+1} - \Theta_i}{6\Delta z}\Phi_{i+1} \tag{A.7}$$

$$\left.\frac{\partial \Theta}{\partial z}\frac{\partial \Phi}{\partial z}\right|_{z=z_i} \cong \frac{\Theta_{i-1} - \Theta_i}{2(\Delta z)^2}\Phi_{i-1} +$$

$$\frac{2\Theta_i - \Theta_{i+1} - \Theta_{i-1}}{2(\Delta z)^2}\Phi_i + \frac{\Theta_{i+1} - \Theta_i}{2(\Delta z)^2}\Phi_{i+1} \tag{A.8}$$

$$\left.\frac{\partial}{\partial z}\left(\frac{\partial \Theta}{\partial z}\Phi\right)\right|_{z=z_i} \cong \frac{\Theta_{i-1} - \Theta_i}{2(\Delta z)^2}\Phi_{i-1} +$$

$$\frac{\Theta_{i-1} - 2\Theta_i + \Theta_{i+1}}{2(\Delta z)^2}\Phi_i + \frac{\Theta_{i+1} - \Theta_i}{2(\Delta z)^2}\Phi_{i+1} \tag{A.9}$$

$$\left.\frac{\partial}{\partial z}\left(\frac{\partial \Theta}{\partial z}\frac{\partial \Phi}{\partial z}\right)\right|_{z=z_i} \cong \frac{-\Theta_{i-1} + \Theta_i}{(\Delta z)^3}\Phi_{i-1}$$

$$\frac{\Theta_{i-1} - \Theta_{i+1}}{(\Delta z)^3}\Phi_i + \frac{\Theta_{i+1} - \Theta_i}{(\Delta z)^3}\Phi_{i+1}. \tag{A.10}$$

REPORT DOCUMENTATION PAGE

Form Approved
OMB No. 0704-0188

1. Agency Use Only *(Leave blank).*	2. Report Date.	3. Report Type and Dates Covered.
	1990	Proceedings

4. Title and Subtitle.
Higher-order and elastic parabolic equations for wave propagation in the ocean

5. Funding Numbers.
Program Element No. 61153N
Project No. 03205
Task No. 330
Accession No. DN257033

6. Author(s).
Michael D. Collins

7. Performing Organization Name(s) and Address(es).
Naval Oceanographic and Atmospheric Research Laboratory*
Stennis Space Center, MS 39529-5004

8. Performing Organization Report Number.
PR 89:025:221

9. Sponsoring/Monitoring Agency Name(s) and Address(es).
Naval Oceanographic and Atmospheric Research Laboratory*
Stennis Space Center, MS 39529-5004

10. Sponsoring/Monitoring Agency Report Number.
PR 89:025:221

11. Supplementary Notes.
*Formerly Naval Ocean Research and Development Activity

12a. Distribution/Availability Statement.
Approved for public release; distribution is unlimited.

12b. Distribution Code.

13. Abstract *(Maximum 200 words).*

A higher-order parabolic equation (PEA) based on a Pade' series [13] and an elastic PE [10] are applied to wave propagation in the ocean. In contrast to the standard PE models of underwater acoustics, the higher-order PE provides accurate solutions for problems involving arbitrarily long ranges, propagation nearly normal to the preferred direction, and large variations in sound speed. The most important applications of the higher-order PE are for problems involving elastic ocean bottoms. A new numerical approach based on centered differences is applied to handle interface conditions. The accuracy of the elastic PE is demonstrated with benchmark calculations. The elastic PE is applied to a range-dependent propagation problem.

14. Subject Terms.
(U) Acoustic Waves; (U) Elastic Waves; (U) Seismic Waves

15. Number of Pages.
18

16. Price Code.

17. Security Classification of Report.	18. Security Classification of This Page.	19. Security Classification of Abstract.	20. Limitation of Abstract.
Unclassified	Unclassified	Unclassified	SAR